This article has been accepted for publication in a future issue of this journal, but has not been fully edited. Content may change prior to final publication. Citation information: DOI 10.1109/JBHI.2017.2664579, IEEE Journal of Biomedical and Health Informatics

# In-silico Modeling of the Functional Role of Reduced Sialylation in Sodium and Potassium Channel Gating of Mouse Ventricular Myocytes

Du, Dongping, Yang, Hui, Ednie, Andrew R. and Bennett, Eric S.

***Abstract*— Cardiac ion channels are highly glycosylated membrane proteins, with up to 30% of the protein's mass containing glycans. Heart diseases often accompany individuals with congenital disorders of glycosylation (CDG). However, cardiac dysfunction among CDG patients is not yet fully understood. There is an urgent need to study how aberrant glycosylation impacts cardiac electrical signaling. Our previous works reported that congenitally reduced sialylation achieved through deletion of the sialyltransferase gene, ST3Gal4, leads to altered gating of voltage-gated $Na^+$ and $K^+$ channels ($Na_v$ and $K_v$, respectively). However, linking the impact of reduced sialylation on ion channel gating to the Action Potential (AP) is difficult without performing computer experiments. Also, decomposing the sum of K+ currents is difficult because of complex structures and components of $K_v$ channels (e.g., $K_v$4.2, and $K_v$1.5). In the present study, we developed in-silico models to describe the functional role of reduced sialylation in both $Na_v$ and $K_v$ gating and the AP using in-vitro experimental data. Modeling results showed that reduced sialylation changes $K_v$ gating as follows: (1) The steady-state activation voltages of $K_v$ isoforms are shifted to a more depolarized potential. (2) Aberrant K+ currents ($I_{Kslow}$ and $I_{to}$) contribute to a prolonged AP duration (APD), and altered Na+ current ($I_{Na}$) contributes to a shortened AP refractory period. This present study contributes to a better understanding of the functional role of reduced sialylation in cardiac dysfunction which shows strong potential to provide new pharmaceutical targets for the treatment of CDG-related heart diseases.**

***Key Words***: Sodium channel, potassium channel, cardiac action potential, reduced sialylation, in-silico modeling, refractory period.

## I. Introduction

The action potential (AP), produced by the orchestrated function of ion channels, represents the change of transmembrane potential as a function of time in a cardiac contraction cycle [1]. A small variation in ion channel activities can influence the AP morphology and electrical conduction, thereby potentially leading to abnormal cardiac electrical signaling and cardiac arrhythmias [2, 3]. Voltage-gated $Na^+$ channels ($Na_v$) and $K^+$ channels ($K_v$) play significant roles in cardiac excitation and conduction. The $Na_v$ contribute greatly to the AP initiation and conduction of the AP across myocardium. Functional changes in $Na_v$ can cause severe cardiac pathologies [4, 5]. Also, $K_v$ produces outward $K^+$ currents throughout many phases of the AP. Such $K^+$ currents play essential roles in either holding the resting potential near the equilibrium or repolarizing the cell [6, 7]. Aberrant $K^+$ channel activities can alter the APs, thereby leading to abnormal cardiac electrical signaling [8-10].

The cardiac ion channel is a glycosylated membrane protein, in which up to 30% of the protein's mass consists of glycan structures [11]. Glycosylation is a common cellular process that contains the coordinated actions of hundreds of unique glycan structures [12]. The dynamic process of glycosylation produces various sets of glycan structures, which impose distinctive mechanisms in cardiac cells [13-17]. It was shown that glycans attached to specific ion channels could have significant effects on cardiac electrical signaling [11]. For example, negatively charged sialic acid residues impact cardiac electrical signaling by directly altering the gating of voltage-gated ion channels [18].

Emerging evidence indicates that congenitally reduced glycosylation may be related to aberrant cardiac electrical signaling. Congenital disorders of glycosylation (CDG) which contains > 40 different types counts for a large portion of pathological states resulting from reduced glycosylation [19]. A typical cause of CDG is the mutation or deficiency in the glyco-associated genes, which leads to relatively modest changes in glycoprotein glycosylation [20, 21]. Cardiac diseases often accompany individuals with CDG. However, cardiac pathologies among all CDG patients and etiology of cardiomyopathy among young patients are not yet fully understood [22-24].

To investigate the impact of aberrant glycosylation on ion channel gating and cardiac function, we measured $Na^+$ currents, $K^+$ currents, and the AP from primarily isolated ventricular apex myocytes using the whole cell patch-clamp recording methods to determine $Na_v$ and $K_v$ isoform biophysical gating parameters as reported by us previously [25-27]. In our experiments, the beta-galactoside alpha-2, 3-sialyltransferase 4 (ST3Gal4) gene, which is uniformly expressed throughout the heart and is responsible for N- and O-linked glycoprotein sialylation, was deleted. Thus, ST3Gal4 gene deletion will result in reduced protein sialylation as shown by us previously for $Na_v$1.5, $K_v$1.5, and $K_v$4.2 [25]. Two datasets were measured, one from wild-type (WT) ventricular apex myocytes and one from apex myocytes isolated from the ST3Gal4$^{-/-}$ ventricle.

Although in-vitro experiments exhibited some changes in ion channels and myocytes for reduced sialylation as reported by us previously [25], detailed understanding of pathological mechanisms across different organizational levels remains ambiguous. In-vitro experiments alone are limited in their

*Research supported by National Science Foundation (CMMI-1646664, CMMI-1646660, CMMI-1619648, CMMI-1617148, and IOS-1660928), and American Heart Association (14GRNT20450148 and 15POST25710010).

D. Du is with the Texas Tech University, Lubbock, TX 79409 USA (e-mail: dongping.du@ttu.edu).

H. Yang is with the Complex Systems Monitoring, Modeling and Control lab, The Pennsylvania State University, University Park, PA, 16802 USA (e-mail: huy25@psu.edu).

A. R. Ednie and E. S. Bennett are with the Department of Neuroscience, Cell Biology and Physiology, Wright State University, Dayton, OH 45435 USA (e-mail: andrew.ednie@wright.edu, eric.bennett@wright.edu).

This article has been accepted for publication in a future issue of this journal, but has not been fully edited. Content may change prior to final publication. Citation information: DOI 10.1109/JBHI.2017.2664579, IEEE Journal of Biomedical and Health Informatics

ability to determine whether functional changes at a lower organizational level (e.g., ion channels) are fully responsible for changes at a higher organizational level (e.g., the cardiomyocyte). For example, in-vitro experiments cannot determine how aberrant changes in $Na_v$ and $K_v$ channels collaboratively lead to the variations in AP waveforms and electrical conduction.

Also, $K_v$ (e.g., Kv4.2, and Kv1.5) activate at a similar range of voltages, thus making it difficult to separate $K^+$ currents experimentally through patch-clamp protocols [28, 29]. Specifically, $K_v$ produces different K+ currents that contribute to various phases of the AP. Patch-clamp experiments can measure the joint $K^+$ current that is a summation of all types of $K^+$ currents flowing through various $K^+$ channels, but not a specific type of $K_v$. However, it is critical to characterize the impact of reduced sialylation on each $K_v$ isoform and their joint effects on the AP. This is conducive to developing a better understanding of pathological changes in CDG-related heart diseases.

Thus, we coupled in-vitro data from electrophysiological experiments with mathematical models to study how reduced sialylation impacts both $K_v$ and $Na_v$ as well as the AP waveform in mouse ventricular apex myocytes. We derived the analytical formulations for the models of $K_v$, and optimally calibrated in-silico models using in-vitro data. Further, we modeled the joint effects of reduced glycosylation on $K_v$ and $Na_v$, and then integrated the channel models with the cell model to predict the AP waveform and refractory period. Notably, the impact of reduced sialylation on cardiac electrical signaling was also studied by varying one factor (i.e., one ion channel) at a time, thereby allowing one to determine how pathological changes in the level of an ion channel contribute to systematic changes at the cellular level.

The paper is organized as follows: Section II presents cardiac models of $K_v$ and $Na_v$, and the ventricular AP; Section III includes the in-vitro data and experimental design. Section IV presents experimental results, which is followed by Section V Conclusions.

## II. Computer Models of $K_v$ and $Na_v$ Isoforms and Cardiac Myocyte

In-silico modeling overcomes practical limitations in in-vitro experimental studies, and provides a descriptive understanding of detailed mechanisms of cardiac pathological function. This present investigation integrated in-vitro data obtained from electrophysiological experiments with in-silico models to investigate the impact of reduced sialylation on specific $K_v$ isoforms that are responsible for the two major repolarizing $K^+$ currents in mouse ventricular apex myocytes, i.e., $I_{Kslow}$ and $I_{to}$, as well as predict their effects on the AP. In addition, in-silico models were developed to investigate the joint effects of reduced sialylation on $K_v$ and $Na_v$ and their collaborative impacts on the AP waveform. In-silico models of $K_v$, $Na_v$, and ventricular myocytes are described as follows.

### *3.1 In-silico modeling of $K_v$*

The repolarization in mouse ventricular cells is predominated by outward $K^+$ currents. The differences between APs in the human ventricle and the mouse ventricle are shown in Figure 1. In human myocytes, the voltage-gated $Na^+$ current ($I_{Na}$) triggers the fast upstroke (phase 0) of AP, which is followed by a transient repolarization (phase 1) to a plateau phase (phase 2). The plateau phase is maintained by the balance of outward $K^+$ currents and inward currents $I_{CaL}$. After the $Ca^{++}$ channels inactivate, the rapid depolarization (phase 3) starts and drives the AP back to the resting potential (phase 4). In mouse ventricular myocytes, there is no clear plateau phase, with the AP upstroke followed by a rapid repolarization induced by the $K^+$ efflux through $K_v$. Our previous study indicated that ST3Gal4 gene deletion does not impact voltage-gated $Ca^{++}$ channel activities [25]. Therefore, the present study focuses on modeling the impact of reduced glycosylation on $K_v$ in mouse ventricular cells.

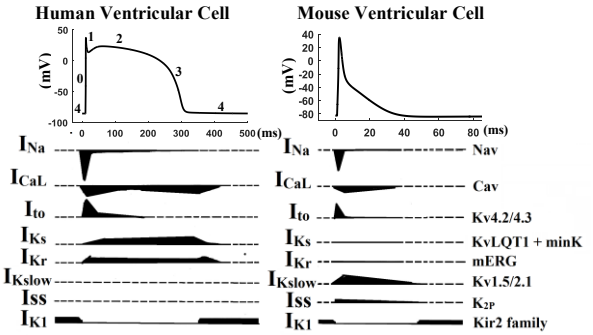


Figure 1. Ion currents and APs in human (left) and mouse (right) ventricular apex myocytes [30].

In mouse ventricular myocytes, there are various types of $K_v$ whose activities are responsible for producing different kinds of $K^+$ currents that contribute to the AP. As shown in Fig. 1, these $K^+$ channels generate $K^+$ currents such as a transient outward potassium current ($I_{to}$), a rapid delayed rectifier potassium current ($I_{Kr}$), a delayed rectifier potassium current $I_{Kslow}$, a slow delayed rectifier potassium current ($I_{Ks}$), a time-independent potassium current ($I_{K1}$), and a non-inactivating current ($I_{ss}$) that is conducted through the non-voltage-dependent "two-pore" type channels ($K_{2P}$) [6, 29, 30]. It may be noted that there are two types of transient outward potassium currents, $I_{to,f}$ and $I_{to,s}$, and $I_{to,s}$ is reported only appearing in ventricular septal myocytes [31]. Here, since all of the experimental data were recorded from ventricular apex myocytes, our efforts will focus on the $I_{to}$ that is produced in apex myocytes, primarily through the activity of $K_v$4.2 [29]. Also, the magnitudes of $I_{Kr}$, $I_{Ks}$ and $I_{K1}$ are small during a mouse AP cycle [30], and our previous study showed that $I_{ss}$ is not impacted by ST3Gal4 expression [25]. However, as illustrated in Fig. 1, $I_{to}$ and $I_{Kslow}$ currents yield larger amplitudes with a bigger impact on cardiac electrical signaling than $I_{Kr}$, $I_{Ks}$ and $I_{K1}$. Thus, in the present study, we focus on development of in-silico models to investigate how reduced sialylation modulates $I_{to}$ ($K_v$4.2 activity) and $I_{Kslow}$ ($K_v$1.5/$K_v$2.1 activity).

This article has been accepted for publication in a future issue of this journal, but has not been fully edited. Content may change prior to final publication. Citation information: DOI 10.1109/JBHI.2017.2664579, IEEE Journal of Biomedical and Health Informatics

In the literature, Markov-based models and Hodgkin-Huxley (HH) models are frequently used to describe ion channel behaviors. Markov models have been used to describe $Na^+$ channel [32], L-type $Ca^{++}$ channel [33], and Rapid delayed rectifier $K^+$ channel [34] behaviors, as well as many other ion channel types. In ventricular myocytes, the transient outward potassium current $I_{to}$ and the delayed rectifier potassium current $I_{Kslow}$ are often modeled using HH type model, as the activations of the channels can be sufficiently captured by the less complicated HH model. For example, Bondarenko et. al model (mouse ventricular model) [33], ten Tusscher et. al model (human ventricular model) [34], and Mahajan et. al model (Rabbit ventricular model) [35] all describe the $I_{to}$ with HH model, which has two independent gating variables of activation and inactivation. In addition, Bondarenko et. al also modeled the $I_{Kslow}$ current using HH type model with an activation variable and an inactivation variable. In this study, we derived the model of $I_{to}$ and $I_{Kslow}$ based on the HH model in Bondarenko et. al mouse ventricular cell model. The equations will be detailed in the following sections.

*Transient outward $K^+$ current* ($I_{to}$): The transient outward potassium current $I_{to}$ includes two components, $I_{to,f}$ and $I_{to,s}$, but $I_{to,s}$ only appears in ventricular septal myocytes. Because ventricular apex myocytes are used in this investigation, we only considered the dominant component of $I_{to}$, i.e., $I_{to,f}$. We calibrated the model of Bondarenko et al [33] to describe how reduced sialylation alters the $I_{to}$ currents. Note that $I_{to}$ is modeled by two gating variables, i.e., activation $a_{to}$ and inactivation $i_{to}$ as follows:

$$I_{to} = G_{Kto} a_{to}^3 i_{to} (V - E_K)$$

where $G_{Kto}$ is the maximum conductance of $I_{to}$ (mS/uF), $a_{to}$ and $i_{to}$ are gating variables, $V$ is the transmembrane potential (mV), and $E_K$ is the reverse potential of K+ channels (i.e., -82.8mV in our in-vitro experiments). Considering the computational complexity, we derived analytical solutions of the gating variables as follows.

$$a_{to}(t) = (a_{to}(0) - a_{ss}) e^{-\frac{t}{\tau_{ato}}} + a_{ss}$$

$$i_{to}(t) = (i_{to}(0) - i_{ss}) e^{-\frac{t}{\tau_{ito}}} + i_{ss}$$

where $a_{to}(0)$ and $i_{to}(0)$ are the initial values, $a_{ss}$ and $i_{ss}$ are the steady state activation (SSA) and steady state inactivation (SSI), $\tau_{ato}$ and $\tau_{ito}$ are activation and inactivation time constants. The detailed models of SSA, SSI, and time constants are listed in Table I.

*Delayed rectifier $K^+$ current* ($I_{Kslow}$): Similar to $I_{to}$, the $I_{Kslow}$ is described by two gating variables of activation $a_r$ and inactivation $i_r$ as:

$$I_{Kslow} = G_{Kslow} a_r i_r (V - E_K)$$

where $G_{Kslow}$ is the maximum conductance of $I_{Kslow}$ (mS/uF), $a_r$ and $i_r$ are gating variables. The two gating variables are modeled as:

$$a_r(t) = (a_r(0) - a_{rs}) e^{-\frac{t}{\tau_{ar}}} + a_{rs}$$

$$i_r(t) = (i_r(0) - i_{rs}) e^{-\frac{t}{\tau_{ir}}} + i_{rs}$$

where $a_r(0)$ and $i_r(0)$ are the initial values, $a_{rs}$ and $i_{rs}$ are steady-state activation and inactivation, $\tau_{ar}$ and $\tau_{ir}$ are time constants of activation and inactivation respectively.

### *3.2 In-silico Modeling of $Na_v$ and Fast $Na^+$ Currents*

The fast Na+ current, $I_{Na}$, is responsible for the rapid depolarization of the ventricular AP. Slightly changes in $Na_v$ may vary the depolarization and the AP refractory period, which can further alter electrical conduction among cardiac tissues. To model the impact of reduced sialylation on the $I_{Na}$, we utilized the 9-state Markov model introduced by Bondarenko et al [33] to describe the gating of $Na_v$ under both WT and ST3Gal4$^{-/-}$ conditions. The model structure is shown in Fig. 2, where $C_1$, $C_2$, $C_3$ are three closed states, IF is fast inactivation, I1, I2 are intermediate inactivated states, O is the open state, and $IC_2$, $IC_3$ are closed-state inactivation. The list of equations and parameters of transition rates, i.e., $\alpha$'s and $\beta$'s in WT and ST3Gal4$^{-/-}$ can be found in our previous report [27]. The $I_{Na}$ model is given:

$$I_{Na} = G_{Na} O(t) (V - E_{Na})$$

where $V$ is the transmembrane potential (mV) of the cardiac myocyte, $G_{Na}$ is the maximum $Na^+$ conductance, $O(t)$ describes the probability of the $Na_v$ activation varying over time $t$, and $E_{Na}$ is the reverse potential (20.5mV).

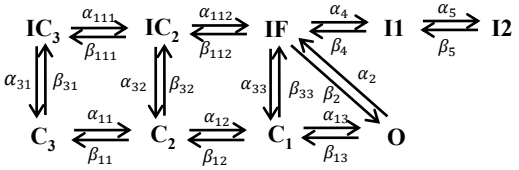


Figure 2. Markov model of gating kinetics of $Na_v$ [27].

### *3.3 In-silico Modeling of Mouse Ventricular Myocyte*

At the cellular level, we simulate the AP in both WT and ST3Gal4$^{-/-}$ conditions. The AP of the ventricular myocyte is modeled as the following ordinal differential equation:

$$-C_m \frac{dV}{dt} = I_{CaL} + I_{p(Ca)} + I_{NaCa} + I_{Cab} + I_{Kslow} + I_{Nab} + I_{Na} + I_{NaK} + I_{K1} + I_{Ks} + I_{to} + I_{ss} + I_{Cl,Ca} + I_{Kr} + I_{stim}$$

where $C_m$ is the membrane capacitance, $t$ is time, $I_{stim}$ is a stimulus current. The ventricular cell model includes 14 transmembrane currents, i.e., the L-type $Ca^{++}$ current ($I_{CaL}$), the $Ca^{++}$ pump current ($I_{p(Ca)}$), the $Na^+/Ca^{++}$ exchange current ($I_{NaCa}$), and the background $Ca^{++}$ ($I_{Cab}$) and $Na^+$ ($I_{Nab}$) currents, the time-independent inwardly rectifying $K^+$ current ($I_{K1}$), the fast $Na^+$ current ($I_{Na}$), the $Na^+/K^+$ pump current ($I_{NaK}$), the slow delayed rectifier $K^+$ current ($I_{Ks}$), the rapid delayed rectifier $K^+$ current ($I_{Kr}$), and the $Ca^{++}$ activated $Cl^-$ current ($I_{Cl,Ca}$). Hodgkin-Huxley type and Markov-based models are used to describe the ionic currents, which includes parameters relating to cell conductance, gating kinetics, and the gradients of membrane potential. Detailed ion-channel gating kinetics can be found in Bondarenko et al [33].

## III. In-vitro Data and Experimental Design

As mentioned, there are various types of $K_v$ isoforms responsible for the total $I_K$ produced in ventricular myocytes,

This article has been accepted for publication in a future issue of this journal, but has not been fully edited. Content may change prior to final publication. Citation information: DOI 10.1109/JBHI.2017.2664579, IEEE Journal of Biomedical and Health Informatics

and it is difficult to separate the $K^+$ currents experimentally using patch clamp protocols. The in-vitro experiments collected the data of the joint $K^+$ currents [25], which needed to be further decomposed to obtain individual $K^+$ currents. This is commonly done through a bi-exponential decomposition. This section will detail how we used both in-vitro data and in-silico models to separate $I_{to}$ and $I_{Kslow}$.

### *4.1 Model-based Decomposition of K+ Currents*

The total $K^+$ current, $I_{K,sum}$, was measured using patch-clamp protocols as reported by us previously[25]. Briefly, the myocytes were first held at -70mV (i.e., the resting membrane potential), and then stepped to various voltages ranging from -50mV to 50mV in 10mV increments. The cells were depolarized for 4.5seconds at each clamp-voltage, and the joint K+ currents, $I_{K,sum}$ were collected. A total of 11 current traces were recorded.

There are various types of $K^+$ currents, and each contributes to the $I_{K,sum}$ currents differently. Note that $I_{Kr}$ and $I_{Ks}$ have very small amplitudes in mouse ventricular myocytes and thus have very limited contribution; $I_{K1}$ has a relatively larger amplitude but is primarily responsible for maintaining the resting potential of the AP. Fig. 1 shows that $I_{to}$, $I_{Kslow}$ and $I_{ss}$ have significantly larger amplitudes. Fig. 3 illustrates the contribution of $I_{to}$, $I_{Kslow}$ and $I_{ss}$ to the trace of $I_{K,sum}$ in a patch-clamp experiment (clamp voltage = 30mV). It may be noted that $I_{to}$ starts at the beginning of the depolarization with a higher peak of magnitude, $I_{Kslow}$ is slightly slower with a lower peak and longer tail, and $I_{ss}$ remains a steady constant after reaching the peak. Such properties of $K^+$ currents enable the separation of $I_{K,sum}$ using a bi-exponential approach, where the decaying portion of the $I_{K,sum}$ is fitted to a bi-exponential function:

$$f(t) = A_1 e^{-t/\tau_1} + A_2 e^{-t/\tau_2} + A_3$$

where $A_1$ is the amplitude of the $I_{Kslow}$ of each $I_{K,sum}$ trace, $A_2$ is the amplitude of the $I_{to}$, $A_3$ is the amplitude of the $I_{ss}$, $t$ is the time in ms, and $\tau_1$ and $\tau_2$ are time constants. The method, as a means to delineate the different $K^+$ currents in mouse ventricular cells, was described previously by Guo et. al [36]. After the decomposition, we obtained the individual $K^+$ currents, i.e., $I_{to}$, $I_{Kslow}$ and $I_{ss}$, at each depolarization, and then characterized and modeled the gating characteristics of each type of $K_v$. Specifically, SSA, SSI, and time constants of inactivation $(t_{inact})$ were determined for $I_{to}$ and $I_{Kslow}$.

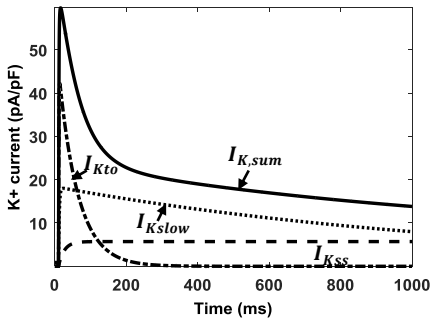


Figure 3. K+ currents at the +30 mV clamp voltage

### *4.2 Design of Computer Experiments*

Computer experiments were designed to model how ST3Gal4$^{-/-}$ affects each individual $K^+$ current type, predict the impact of changes in $K^+$ currents and $Na^+$ currents on the AP, and identify the contribution of each type of current to aberrant electrical signaling in ventricular myocytes. *First*, we modified and calibrated the model of $K_v$ gating to optimally fit the in-vitro data. The current density, SSA and SSI, and inactivation time constants were obtained using the same protocols as in the in-vitro experiments. *Second*, we simulated and compared the changes in $K^+$ currents and the cellular APs under two conditions, i.e. WT vs. ST3Gal4$^{-/-}$. *Third*, we combined the effects of ST3Gal4$^{-/-}$ on $Na_v$ and $K_v$ isoforms and then predicted the AP at the cellular level. Meanwhile, specific contributions of each individual current, i.e., $I_{to}$, $I_{Kslow}$ and $I_{Na}$, to the changes in AP were evaluated. The time step of $dt$ = 0.01ms was used in computer experiments for the model calibration at the channel level. Variable time steps with maximum step time of 0.1ms were used in the experiments at the cellular level, where each cell was stimulated for 40 times to reach the stable phase.

Computer simulations were implemented in MATLAB R2015a in a Windows 7 Enterprise 64-bit Operating System. Computer experiments were designed following the same protocols used for in-vitro experiments to calibrate in-silico models and to compute the model responses. The models of mouse ventricular cells, as well as $K_v$ and $Na_v$ isoforms, were solved using Matlab's ode15s solver, and the maximal step size is set at 0.1ms.

## IV. Experimental Results

### *5.1 Sensitivity Analysis and Control Variables*

In order to identify the model parameters that exert the most influence on model outputs, we performed a sensitivity analysis using factorial design. Each parameter varied at two levels (+1 and -1), and the model outputs of SSA, SSI, and Inactivation time constants were calculated to obtain factorial effects. The impacts of model parameters on model outputs were evaluated using the factorial effects and half-normal plot (See details in the online supplement A). Sensitivity analysis provides important parameters (i.e., control variables) in $I_{to}$ model and $I_{Kslow}$ model, respectively. The detailed mathematical formulations of steady-state activation, inactivation, transition rates, and time constants are listed in Table I. Note that $\boldsymbol{x's}$ are control variables identified from sensitivity analysis, which will be optimally calibrated to minimize the discrepancy of modeled outputs and in-vitro data. These control variables are closely pertinent to voltage ($V$), e.g., $\boldsymbol{x}_1$ and $\boldsymbol{x}_3$. Steady state activation and inactivation of $I_{Kslow}$ and $I_{to}$ channels were calibrated using data from Boltzmann equations of WT and ST3Gal4$^{-/-}$ cells in in-vitro experiments. In addition, time constant $\tau$'s were calibrated to fit the data from in-vitro experiments.

This article has been accepted for publication in a future issue of this journal, but has not been fully edited. Content may change prior to final publication. Citation information: DOI 10.1109/JBHI.2017.2664579, IEEE Journal of Biomedical and Health Informatics

TABLE I. $K_V$ MODELS AND CONTROL VARIABLES

| Steady States, Transition Rates & Time Constant | |
|---|---|
| $a_{ss}$ | = 1/(1+exp(-(V-$x_1$)/ $x_2$)) |
| $i_{ss}$ | = 1/(1+exp(-(V-$x_3$)/ $x_4$)) |
| $\tau_{ato}$ | = $1/(\alpha_a+\beta_a)$ |
| $\tau_{ito}$ | = $1/(\alpha_i+\beta_i)$ |
| $\alpha_a$ | = 0.1807 exp ( 0.0358 ($V$+40.0)) |
| $\beta_a$ | = 0.3956 exp (-0.0624($V$+40.0)) |
| $\alpha_i$ | = (0.000152 exp(-($V$+13.5)/7.0))/(0.067083exp(-($V$+33.5)/7.0)+1) |
| $\beta_i$ | = (0.000950 exp(-($V$+ $x_5$ )/$x_6$))/(0.051335exp( ($V$+ $x_5$ )/ $x_6$)+1) |
| $a_{rs}$ | = 1/(1+ exp(-($V$-$x_7$)/$x_8$)) |
| $i_{rs}$ | = 0.2100/(1+exp(-($V$-$x_9$)/ $x_{10}$)+0.7900/(1+exp(-($V$-$x_{11}$)/ $x_{12}$) |
| $\tau_{ir}$ | = 500.0+$x_{13}$ (1+ exp (($V$+$x_{14}$)/0.0492))$^{-1}$ |
| $\tau_{ar}$ | = 0.4930exp (-0.0629$V$) +$x_{15}$ |

## 5.2 Model Calibration of $K_v$ isoforms

We used the algorithm of constrained nonlinear optimization (i.e., trust-region method) to search the optimal set of model parameters. The objective function is to minimize the sum of squared errors between the model predictions and the in-vitro data. Table II shows optimal values of control variables in the two groups, i.e., WT vs. ST3Gal4$^{-/-}$. Note that optimal parameters of WT and ST3Gal4$^{-/-}$ models are different in half-activation and half-inactivation voltage as well as slope factors. The calibration step yields the best fits of in-silico models to the WT and ST3Gal4$^{-/-}$ experimental data using the same set of standard pulse protocols.

TABLE II. OPTIMAL MODEL PARAMETERS OF WT AND ST3GAL4$^{-/-}$ $K_V$

| | WT (mV) | ST3Gal4$^{-/-}$ (mV) | | WT (mV) | ST3Gal4$^{-/-}$ (mV) |
|---|---|---|---|---|---|
| $x_1$ | -0.30 | 7.40 | $x_9$ | -81.46 | -83.73 |
| $x_2$ | 12.00 | 14.00 | $x_{10}$ | -5.98 | -7.86 |
| $x_3$ | -37.40 | -36.20 | $x_{11}$ | -34.31 | -32.64 |
| $x_4$ | -4.10 | -4.90 | $x_{12}$ | -4.31 | -6.36 |
| $x_5$ | 85.13 | 121.43 | $x_{13}$ | 633.36 | 828.67 |
| $x_6$ | 24.55 | 39.87 | $x_{14}$ | -13.79 | -5.09 |
| $x_7$ | -14.70 | -7.80 | $x_{15}$ | 2.058 | 2.060 |
| $x_8$ | 8.20 | 9.60 | | | |

## 5.3 ST3Gal4-/- Alters the Activities of Kv

*Transient outward K$^+$ current ($I_{to}$):* We modeled the gating kinetics of $I_{to}$ channels, see Tables I and II. Fig. 4 presents the SSA and SSI of $I_{to}$ in both in-vitro and in-silico experiments. Note that ST3Gal4$^{-/-}$ causes a small depolarized shift (~7mV) in SSA. However, no significant difference is observed in SSI between the two groups except the slight difference at the -30mV test potential. Fig. 5a shows the current density of $I_{to}$, where ST3Gal4$^{-/-}$ causes a significant reduction at membrane potentials greater than 20mV. The amplitude of $I_{to}$ at 40mV is 21.70pA/pF in the WT cell and 17.32pA/pF in ST3Gal4$^{-/-}$, which are within the range of the in-vitro data (see Table III), i.e., 21.6±2.0pA/pF in WT and 17.4±1.6pA/pF in ST3Gal4$^{-/-}$ myocytes [25]. The observed reduction in current density is likely caused by the depolarizing shift in the activation (Fig. 4a), and no impact on inactivation gating (Fig. 4b), because the range of membrane potentials at which the $I_{to}$ channel activates is reduced. In the $I_{to}$ current model, we used a maximum conductance $G_{to}$ = 0.19 (mS/uF) for WT cells, and $G_{to}$ = 0.16 (mS/uF) for ST3Gal4$^{-/-}$ cells, which are close (within the range of standard errors) to in-vitro data (i.e., WT: 0.18±0.0.02; ST3Gal4$^{-/-}$: 0.15±0.02). Computer models describe and predict gating activities and current densities of $I_{to}$, which are well-validated with in-vitro data.

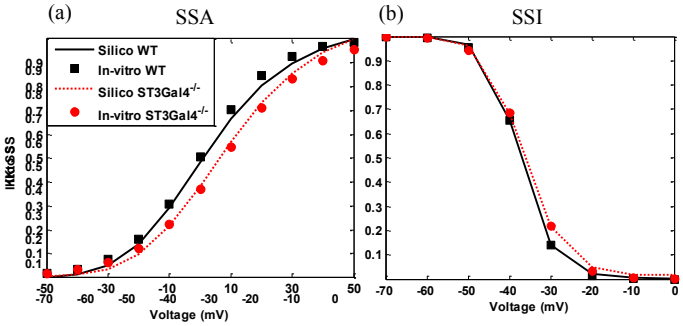


Figure 4. The gating kinetics of $I_{to}$ channel in ST3Gal4$^{-/-}$ and WT cells (a) SSA (b) SSI. (In-silico data from the $I_{to}$ model: solid lines-WT, dashed lines-ST3Gal4$^{-/-}$; In-vitro data: ■WT ● ST3Gal4$^{-/-}$[25]).

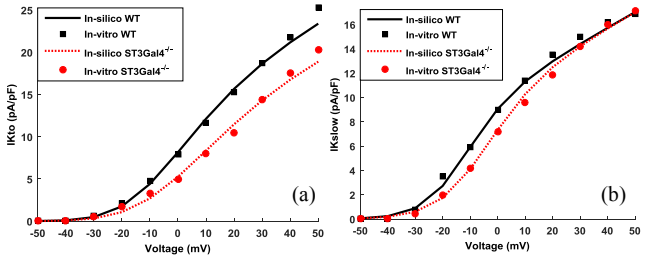


Figure 5. The current-density relationship of $I_{to}$ (a) and $I_{Kslow}$ (b) under ST3Gal4$^{-/-}$ and WT conditions. (In-silico data from computer models: solid lines-WT, dashed lines-ST3Gal4$^{-/-}$; In-vitro data: ■WT ● ST3Gal4$^{-/-}$[25])

TABLE III. CURRENT-DENSITY AND INACTIVATION TIME CONSTANTS OF K+ CURRENTS IN WT AND ST3GAL4$^{-/-}$ MYOCYTES

| | $I_{to}$ | | $I_{Kslow}$ | |
|---|---|---|---|---|
| | (pA/pF) 40mV | $\tau_{inact}$ 40mV | (pA/pF) 40mV | $\tau_{inact}$ 40mV |
| In-silico WT | 21.70 | 60.48 | 15.72 | 1246 |
| In-silico ST3Gal4$^{-/-}$ | 17.32 | 72.40 | 15.66 | 1092 |
| In-vitro WT | 21.6±2.0 | 62.6±3.9 | 16.2±1.6 | 1089±54 |
| In-vitro ST3Gal4$^{-/-}$ | 17.4±1.6 | 71.1±4.3 | 16.0±1.7 | 1270±55 |

*Delayed rectifier K$^+$ current ($I_{Kslow}$)*: The in-silico model of $K_v$ gating showed that the ST3Gal4$^{-/-}$ causes a small rightward shift in the SSA of $I_{Kslow}$ current along the voltage axis (see Fig. 6a), but the SSI of $I_{Kslow}$ is not significantly affected (see Fig. 6b). The results of in-silico modeling are consistent with the in-vitro data (solid dots and squares in Fig. 6), in which ST3Gal4$^{-/-}$ shifts the SSA linearly in the depolarized direction, and has little impact on inactivation. To further investigate how reduced sialylation alters the $K_v$ gating activities and the K$^+$ current, the current density of $I_{Kslow}$ was computed (see Fig. 5b). We used the maximum conductance $G_{Kslow}$=0.13 (mS/uF) for both WT and ST3Gal$^{-/-}$ groups, which is consistent with the in-vitro data (i.e., WT: 0.13±0.01 vs ST3Gal4$^{-/-}$: 0.12±0.02 mS/uF). Table III shows the comparison between in-silico current densities and in-vitro data [25] at a 40mV test potential, where the amplitude of in-silico $I_{Kslow}$ at 40mV is 15.72pA/pF in WT and 15.66pA/pF in ST3Gal4$^{-/-}$ compared to the in-vitro results of

This article has been accepted for publication in a future issue of this journal, but has not been fully edited. Content may change prior to final publication. Citation information: DOI 10.1109/JBHI.2017.2664579, IEEE Journal of Biomedical and Health Informatics

16.2±1.6pA/pF in WT and 16.0±1.7pA/pF in ST3Gal4$^{-/-}$. Note that in-silico results closely match in-vitro data. ST3Gal4$^{-/-}$ contributes to the decrease of $I_{Kslow}$ densities at the range of smaller, non-saturating membrane potentials (i.e., -30mV~20mV).

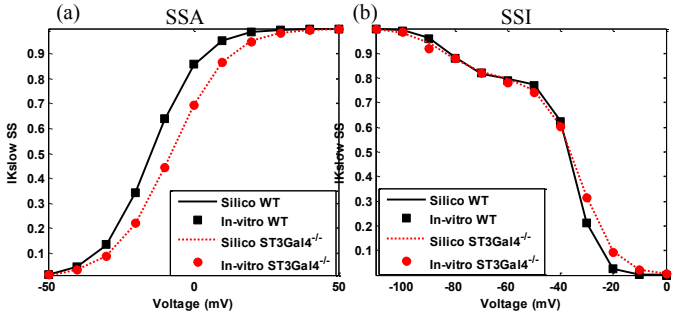


Figure 6. The gating kinetics of $I_{Kslow}$ channel in ST3Gal4$^{-/-}$ and WT cells. (a) SSA (b) SSI. (In-silico data from the $I_{Kslow}$ model: solid lines-WT, dashed lines-ST3Gal4$^{-/-}$. In-vitro data: ■WT ● ST3Gal4$^{-/-}$[25])

*Time constants of inactivation* ($\tau_{inact}$): Fig. 7 shows the in-silico results of time constants $\tau_{inact}$ of $I_{to}$ and $I_{Kslow}$, where $I_{to}$ shows smaller time constants than $I_{Kslow}$ with slight difference between WT and ST3Gal4$^{-/-}$ groups. The $I_{Kslow}$ shows larger time constants with significant differences between the two groups. The in-silico time constant $\tau_{inact}$ of $I_{to}$ at the depolarizing potential of 40mV is 60.48ms and 72.40 ms for WT and ST3Gal4$^{-/-}$ myocytes, respectively. The in-silico results match in-vitro data, i.e., $\tau_{inact}$ is 62.9±3.6ms in WT and 71.1±4.1ms in ST3Gal4$^{-/-}$ (also see Table III). However, $I_{Kslow}$ has a larger $\tau_{inact}$ than $I_{to}$. At the clamp voltage of 40mV, $\tau_{inact}$ of $I_{Kslow}$ is 1092ms (1089 ±54ms of in-vitro data) for WT cells, and 1246ms (1270 ±55ms of in-vitro data) for ST3Gal4$^{-/-}$ cells (Table III). The in-silico results show $\tau_{inact}$ of $I_{to}$ and $I_{Kslow}$ are close to the in-vitro data, which validates the performance of in-silico models at the level of ion channels.

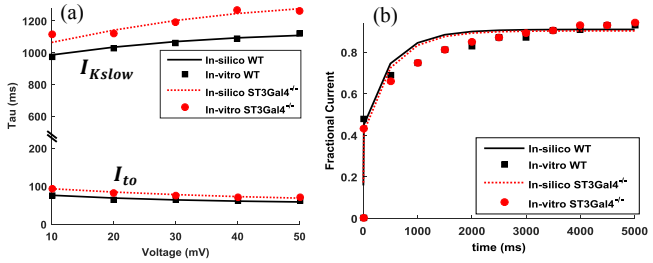


Figure 7 (a) Inactivation time constants of $I_{Kslow}$ and $I_{to}$ under ST3Gal4$^{-/-}$ and WT conditions; (b) Recovery from inactivation under WT and ST3Gal4$^{-/-}$ conditions. (In-silico data from computer models: solid lines-WT, dashed lines-ST3Gal4$^{-/-}$, In-vitro data: ■WT ● ST3Gal4$^{-/-}$ [25]).

*Recovery from inactivation*: Fig. 7b shows the recovery from inactivation of the joint $K^+$ current, $I_{K,sum}$, generated using the standard two-pulse protocol. In-silico cells were held at a membrane potential of -70mV and depolarized to +40mV for 10s. The in-silico cells were then returned to -70mV for variant time intervals of 10ms to 5s and then depolarized to +40mV for 4.5s. As shown in Fig. 7b, there are no significant differences between the recovery from inactivation in both WT and ST3Gal4$^{-/-}$ groups, which indicates reduced sialylation doesn't not affect $K_v$ recovery from inactivation. This finding matches the in-vitro data (solid dots and squares in Fig. 7b), which also validates the accuracy of $K_v$ models

### 5.4 *ST3Gal4$^{-/-}$ Affects Ventricular Myocyte APs*

*Reduced Sialylation alters $K_v$ activities and delays the AP repolarization.* We combined the calibrated models of $K_v$ isoforms with the ventricular myocyte model to predict the effects of reduced sialylation on $K_v$ activities and the electrical signaling in the ventricular myocyte. Fig. 8 shows the $K^+$ currents, $I_{to}$ and $I_{Kslow}$, in a single cardiac cycle as well as the AP for both WT and ST3Gal4$^{-/-}$ ventricular myocytes.

Fig. 8a shows that both $I_{to}$ and $I_{Kslow}$ have lower peaks and slightly longer tails in ST3Gal4$^{-/-}$ compared to WT. The lower peaks are attributed to the rightward shift of $I_{to}$ and $I_{Kslow}$ SSA curves and no effect on SSI curves (Fig. 4 and Fig. 6), resulting in a smaller range of membrane potentials at which $K_v$ are activated. Because $K_v$ are responsible for AP repolarization, the limited activities of $K_v$ lead to a delayed repolarization (Fig. 8c). It may also be noted that such a delayed repolarization is likely responsible for the longer tails in both $I_{to}$ and $I_{Kslow}$ of ST3Gal4$^{-/-}$ myocytes. The delay of early repolarization caused by lower peaks of $K^+$ currents further generate feedback effects on $I_{to}$ and $I_{Kslow}$, and lead to the prolonged tails in both currents (Fig. 8a and 8b).

Limited $K_v$ activities in ST3Gal4$^{-/-}$ cells lead to longer AP durations (APDs) compared to WT cells (Fig. 8c). Table IV shows a detailed list of AP parameters in the in-silico WT and ST3Gal4$^{-/-}$ myocytes with $K_v$ altered by reduced sialylation. Computer experiments show no significant differences in peaks between the two groups. However, the APDs are prolonged significantly in ST3Gal4$^{-/-}$ cells. As shown in Table IV, the APD at 90% repolarization ($APD_{90}$) is 25.77ms in WT and 35.21ms in ST3Gal4$^{-/-}$. Similarly, the $APD_{75}$ is increased from 16.79ms (WT) to 23.69ms (ST3Gal4$^{-/-}$) and the $APD_{50}$ is increased from 10.49ms (WT) to 14.24ms (ST3Gal4$^{-/-}$).

*ST3Gal4$^{-/-}$ affects both depolarization and repolarization of ventricular AP.* We further integrated the calibrated $K_v$ and $Na_v$ models with the ventricular myocyte model to predict the effects of ST3Gal4$^{-/-}$ on $K_v$ and $Na_v$ and their collaborative effects on the AP. Because $Na_v$ mainly contributes to AP depolarization and cellular excitation, we investigated the refractory period of AP in both WT and ST3Gal4$^{-/-}$ cells. The stimulation currents used in computer experiments to initiate the AP are 54.6pA/pF and 52.0pA/pF for 2.5ms for the WT and ST3Gal4$^{-/-}$ groups, respectively. As shown in Fig. 9, the WT myocyte can recover and excite the second AP after 139.1ms (see the black-solid line in Fig. 9), whereas the ST3Gal4$^{-/-}$ cell can initiate the second AP earlier at 109.2ms (see the red dotted line in Fig. 9). Note that the in-silico results of refractory periods yield an accurate prediction of the in-vitro data as reported in [25], i.e., WT: 139.8 ± 8.6ms, ST3Gal4$^{-/-}$: 110.2 ± 10.0, which cross-validate the in-silico

This article has been accepted for publication in a future issue of this journal, but has not been fully edited. Content may change prior to final publication. Citation information: DOI 10.1109/JBHI.2017.2664579, IEEE Journal of Biomedical and Health Informatics

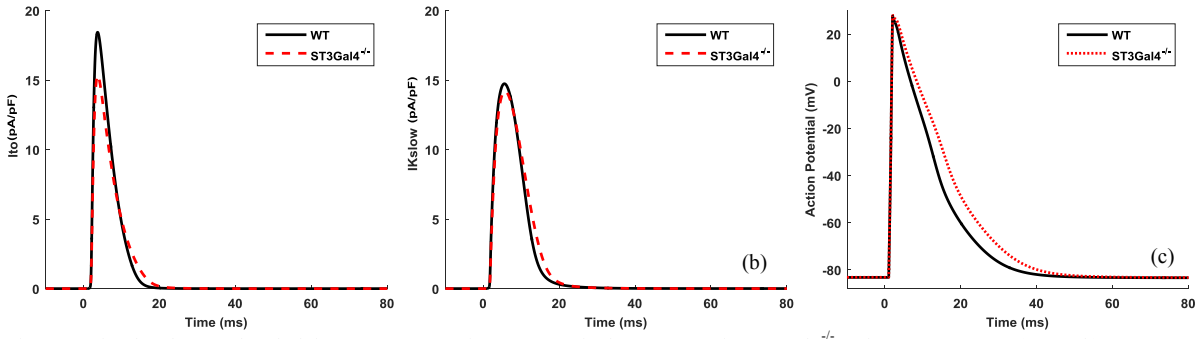


Figure 8. Simulated AP and underlying K+ currents of mouse ventricular myocytes in ST3Gal4$^{-/-}$ and WT myocytes. (a): $I_{to}$. (b): $I_{Kslow}$. (c): AP. Black solid line: WT. Red dash line: ST3Gal4$^{-/-}$.

models. Experimental results demonstrated the effectiveness of in-silico models to describe the mechanistic details of $K_v$ and $Na_v$ gating and to predict the hidden effects of reduced sialylation on ion channels and on the electrical signaling of ventricular myocytes.

TABLE IV. APDS IN WT AND ST3GAL4$^{-/-}$ CELLS IN IN-SILICO AND IN-VITRO DATA

| | $APD_{25}$ | $APD_{50}$ | $APD_{75}$ | $APD_{90}$ | Peak |
|---|---|---|---|---|---|
| **Parameters of modeled AP in WT cells** | | | | | |
| Modeled WT | 4.90 | 10.49 | 16.79 | 25.77 | 27.67mV |
| **Parameters of modeled AP with $K_v$ altered by ST3Gal4$^{-/-}$** | | | | | |
| ST3Gal4$^{-/-}$ $K_v$ | 6.81 | 14.24 | 23.69 | 35.21 | 28.44mV |
| **Parameters of modeled AP with $K_v$ and $Na_v$ altered by ST3Gal4$^{-/-}$** | | | | | |
| ST3Gal4$^{-/-}$ | 6.90 | 14.26 | 23.77 | 35.29 | 28.09mV |
| **In-vitro Data [25]** | | | | | |
| WT | 9.1±0.5 | 11.6±1.0 | 16.4±1.9 | 25.8±3.0 | 27.5±5.1 |
| ST3Gal4$^{-/-}$ | 11.1±0.6 | 15.1±1.0 | 21.8±1.5 | 36.9±2.3 | 27.9±3.9 |

To further identify the causes of a shortened refectory period, we exclude the effects of ST3Gal4$^{-/-}$ on $Na_v$ and solely test how ST3Gal4$^{-/-}$ alters the $K_v$ and the resulting effects on the refractory period. Fig. 9 shows the refractory period of the ST3Gal4$^{-/-}$ cell in which only $K_v$ are modified by ST3Gal4$^{-/-}$ (see the blue dash-dot line). Note that the ST3Gal4$^{-/-}$($K_v$) cell excites the second AP at 134.2ms, which is not significantly different from the WT cell (i.e., 139.1ms). Therefore, the contribution of $K_v$ to the reduced refractory period is very limited in ST3Gal4$^{-/-}$ myocytes. In summary, the effects of ST3Gal4$^{-/-}$ on cardiac excitation is mainly due to the altered gating of $Na_v$.

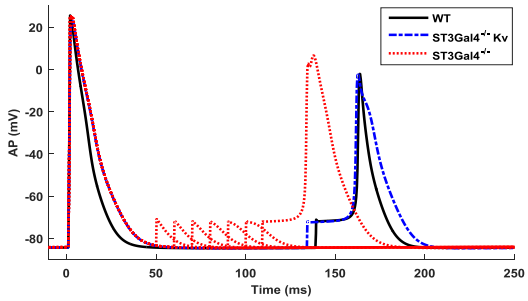


Figure 9. The in-silico refractory period of mouse ventricular myocyte. Red dotted line: ST3Gal4$^{-/-}$ cell (109.2ms); Blue dash-dot line: $K_v$ altered by ST3Gal4$^{-/-}$ (134.2ms); Black line: WT cell (139.1ms)

Also, we compared the APDs of the ventricular myocyte with and without $Na_v$ channel affected by ST3Gal4$^{-/-}$. As shown in Table IV, the APDs at 25%, 50%, 75% and 90% repolarization are almost identical between ST3Gal4$^{-/-}$($K_v$) and the ST3Gal4$^{-/-}$ myocytes. This shows that the variations in the repolarization of AP mainly resulted from altered gating of $K_v$, with little contribution from the effects of reduced sialylation on $Na_v$ gating.

### 5.5 *Model Justification and Validation*

The glycosylation models were developed from Hodgkin-Huxley models of cardiac ion channels and cells. The ventricular myocyte was treated as an electrical circuit, and $K_v$ were described as electrical conductors. The ion currents through the $K_v$ were determined by the intra- and extracellular ionic concentrations $E_K$. The conductance was computed as a function of maximum conductance (i.e. $G_K$) and the open probability of hypothetical gates (i.e. the activation and inactivation variables). The glycosylation model is valid when the assumptions of the Hodgkin-Huxley model hold. In addition, the glycosylation models were developed and validated using the in-vitro data measured from the left ventricular apex of ST3Gal4$^{-/-}$ adult mice. They are efficient in describing the impact of reduced sialylation on $K^+$ currents in mouse ventricular myocytes, but calibration of model parameters may be required for a different congenital disorder or for myocytes from subjects other than mouse.

The in-vitro data indicated that reduced sialylation leads to linear shifts in SSA along the voltage axis [25]. Such changes can limit $K_v$ activities without decreasing the maximal $K^+$ current densities. The limited $K_v$ activities can be modeled by adjusting the open probabilities of the channel of interest, thereby, reducing the channel conductance. Therefore, the impact of reduced sialylation can be captured by optimally calibrating the gating variables in $K_v$ models to match the in-vitro data. The model predictions (i.e., SSA, SSI, inactivation time constants) show good fits to the in-vitro data at the ion channel scale. Further, the well-calibrated channel models were integrated with cellular models. The modeling results at cellular scale match the in-vitro data in our previous reports [25, 26], which validates the model efficiency in interpreting the impact of reduced sialylation on cardiac electrical signaling.

## V. CONCLUSIONS

Computer modeling and experiments have been integrated

This article has been accepted for publication in a future issue of this journal, but has not been fully edited. Content may change prior to final publication. Citation information: DOI 10.1109/JBHI.2017.2664579, IEEE Journal of Biomedical and Health Informatics

with in-vitro studies for decades to investigate disease-altered cardiac electrical signaling. Electrophysiology experiments alone are limited in their ability to develop a complete understanding on how reduced sialylation modulates the function of ion channels and cardiomyocytes. In particular, it is difficult for in-vitro experiments to determine whether a change at one organizational level (e.g., ion channels), is responsible for the change at a higher organizational level (e.g., the cardiomyocyte). In-silico studies provide a greater level of flexibility to derive and test new hypotheses, suggest new experimental designs, and overcome practical limitations of in-vitro experiments.

CDG patients have a higher level of risk for heart disease. However, cardiac dysfunction among all CDG patients and etiology of cardiomyopathy among young patients are not yet fully understood. Very little has been done to integrate computer modeling with in-vitro experiments to investigate how aberrant glycosylation affects cardiac function across different organizational levels such as ion channels and cells. This paper couples in-vitro data with in-silico models to study, mechanistically, how congenitally reduced sialylation impacts ion channel gating and cardiac electrical signaling.

We calibrated mathematical models of ion channels and ventricular apex myocytes to describe the effects of reduced sialylation on $Na_v$ and $K_v$ activities, and further predict the impact of ST3Gal4 gene deletion on cardiac electrical signaling. The in-silico study facilitates a better understanding of the functional role of reduced sialylation in $Na_v$ and $K_v$ gating of mouse ventricular myocytes. ST3Gal4 deletion leads to a loss of $K_v4.2$ and $K_v1.5$ sialylation, which contributes to changes in $I_{to}$ and $I_{Kslow}$, respectively. Experimental results in the present investigation showed that ST3Gal4 deletion causes a rightward shift in the SSA of $I_{to}$ and $I_{Kslow}$, but has no effect on SSI. Most importantly, in-silico studies attribute the changes in ST3Gal4$^{-/-}$ myocytes, i.e., the prolonged APDs and the shortened refractory period, predominately to altered gating of $K_v$ and $Na_v$, respectively. Our experimental results suggested that limited $K_v$ activities are responsible for the prolonged APDs, and the altered gating of $Na_v$ contributes to shortened refractory period. This cannot be otherwise achieved through in-vitro experiments. While our efforts here indicate that significant effects of reduced sialylation on myocyte electrical signaling can be described by direct effects on $Na_v$ and some $K_v$ isoforms, the AP could be affected by other ionic elements and future studies will be designed to investigate whether reduced sialylation impacts activity of other channels and transport proteins.

Aberrant glycosylation alters the gating kinetics of ion channels, hence affects cardiac electrical signaling at higher organizational levels, e.g., cells and tissues. The present study provides detailed pathological mechanisms of sialylation modulation dynamics in cardiomyocytes. This will potentially lead to new therapeutic designs to correct aberrant glycosylation and to resume normal cardiac function.

## ACKNOWLEDGMENTS

The authors would like to thank Dr. Randall L. Rasmusson from the Department of Physiology and Biophysics, School of Medicine and Biomedical Sciences, University at Buffalo, State University of New York, USA, for sharing the computer model of action potential of mouse ventricular myocytes.

## REFERENCES

[1] A. O. Grant, "Cardiac ion channels," *Circ Arrhythm Electrophysiol,* vol. 2, pp. 185-94, Apr 2009.
[2] D. J. Beuckelmann, M. Nabauer, and E. Erdmann, "Alterations of K+ currents in isolated human ventricular myocytes from patients with terminal heart failure," *Circ Res,* vol. 73, pp. 379-85, Aug 1993.
[3] M. Nabauer and S. Kaab, "Potassium channel down-regulation in heart failure," *Cardiovasc Res,* vol. 37, pp. 324-34, Feb 1998.
[4] C. A. Remme and C. R. Bezzina, "Sodium channel (dys)function and cardiac arrhythmias," *Cardiovasc Ther,* vol. 28, pp. 287-94, Oct 2010.
[5] J. R. Balser, "The cardiac sodium channel: gating function and molecular pharmacology," *J Mol Cell Cardiol,* vol. 33, pp. 599-613, Apr 2001.
[6] D. J. Snyders, "Structure and function of cardiac potassium channels," *Cardiovasc Res,* vol. 42, pp. 377-90, May 1999.
[7] K. K. Deal, S. K. England, and M. M. Tamkun, "Molecular physiology of cardiac potassium channels," *Physiol Rev,* vol. 76, pp. 49-67, Jan 1996.
[8] G. W. Abbott, "Molecular mechanisms of cardiac voltage-gated potassium channelopathies," *Curr Pharm Des,* vol. 12, pp. 3631-44, 2006.
[9] M. Tristani-Firouzi, J. Chen, J. S. Mitcheson, and M. C. Sanguinetti, "Molecular biology of K(+) channels and their role in cardiac arrhythmias," *Am J Med,* vol. 110, pp. 50-9, Jan 2001.
[10] U. Ravens and E. Cerbai, "Role of potassium currents in cardiac arrhythmias," *Europace,* vol. 10, pp. 1133-7, Oct 2008.
[11] A. R. Ednie and E. S. Bennett, "Modulation of voltage-gated ion channels by sialylation," *Compr Physiol,* vol. 2, pp. 1269-301, Apr 2012.
[12] M. L. Montpetit, P. J. Stocker, T. A. Schwetz, J. M. Harper, S. A. Norring, L. Schaffer, *et al.*, "Regulated and aberrant glycosylation modulate cardiac electrical signaling," *Proc Natl Acad Sci U S A,* vol. 106, pp. 16517-22, Sep 22 2009.
[13] P. J. Stocker and E. S. Bennett, "Differential sialylation modulates voltage-gated Na+ channel gating throughout the developing myocardium," *J Gen Physiol,* vol. 127, pp. 253-65, Mar 2006.
[14] G. Shi and J. S. Trimmer, "Differential asparagine-linked glycosylation of voltage-gated K+ channels in mammalian brain and in transfected cells," *J Membr Biol,* vol. 168, pp. 265-73, Apr 1 1999.
[15] R. A. Schwalbe, M. J. Corey, and T. A. Cartwright, "Novel Kv3 glycoforms differentially expressed in adult mammalian brain contain sialylated N-glycans," *Biochem Cell Biol,* vol. 86, pp. 21-30, Feb 2008.
[16] J. Nacher, R. Guirado, E. Varea, G. Alonso-Llosa, I. Rockle, and H. Hildebrandt, "Divergent impact of the polysialyltransferases ST8SiaII and ST8SiaIV on polysialic acid expression in immature neurons and interneurons of the adult cerebral cortex," *Neuroscience,* vol. 167, pp. 825-37, May 19 2010.
[17] I. K. Vijay, "Developmental and hormonal regulation of protein N-glycosylation in the mammary gland," *J Mammary Gland Biol Neoplasia,* vol. 3, pp. 325-36, Jul 1998.
[18] X. Chen and A. Varki, "Advances in the biology and chemistry of sialic acids," *ACS Chem Biol,* vol. 5, pp. 163-76, Feb 19 2010.
[19] J. Jaeken, "Congenital disorders of glycosylation," *Ann N Y Acad Sci,* vol. 1214, pp. 190-8, Dec 2010.
[20] H. H. Freeze, E. A. Eklund, B. G. Ng, and M. C. Patterson, "Neurology of inherited glycosylation disorders," *Lancet Neurol,* vol. 11, pp. 453-66, May 2012.
[21] S. E. Sparks and D. M. Krasnewich, "Congenital Disorders of N-linked Glycosylation Pathway Overview," in *GeneReviews(R)*, R. A. Pagon, M. P. Adam, H. H. Ardinger, S. E. Wallace, A. Amemiya, L. J. H. Bean, *et al.*, Eds., ed Seattle (WA), 1993.
[22] E. J. Footitt, A. Karimova, M. Burch, T. Yayeh, T. Dupre, S. Vuillaumier-Barrot, *et al.*, "Cardiomyopathy in the congenital disorders

of glycosylation (CDG): a case of late presentation and literature review," *J Inherit Metab Dis,* vol. 32 Suppl 1, pp. S313-9, Dec 2009.
[23] J. Gehrmann, K. Sohlbach, M. Linnebank, H. J. Bohles, S. Buderus, H. G. Kehl, *et al.*, "Cardiomyopathy in congenital disorders of glycosylation," *Cardiol Young,* vol. 13, pp. 345-51, Aug 2003.
[24] M. Al-Owain, S. Mohamed, N. Kaya, A. Zagal, G. Matthijs, and J. Jaeken, "A novel mutation and first report of dilated cardiomyopathy in ALG6-CDG (CDG-Ic): a case report," *Orphanet J Rare Dis,* vol. 5, p. 7, 2010.
[25] A. R. Ednie and E. S. Bennett, "Reduced sialylation impacts ventricular repolarization by modulating specific K+ channel isoforms distinctly," *J Biol Chem,* vol. 290, pp. 2769-83, Jan 30 2015.
[26] A. R. Ednie, K. K. Horton, J. Wu, and E. S. Bennett, "Expression of the sialyltransferase, ST3Gal4, impacts cardiac voltage-gated sodium channel activity, refractory period and ventricular conduction," *J Mol Cell Cardiol,* vol. 59, pp. 117-27, Jun 2013.
[27] D. Du, H. Yang, H. Yang, A. Ednie, and E. Bennett, "Statistical Metamodeling and Sequential Design of Computer Experiments to Model Glyco-altered Gating of Sodium Channels in Cardiac Myocytes," *IEEE J Biomed Health Inform,* vol. 20, pp. 1439-1452, Jul 22 2015.
[28] D. M. Roden and A. L. George, Jr., "Structure and function of cardiac sodium and potassium channels," *Am J Physiol,* vol. 273, pp. H511-25, Aug 1997.
[29] J. Brouillette, R. B. Clark, W. R. Giles, and C. Fiset, "Functional properties of K+ currents in adult mouse ventricular myocytes," *J Physiol,* vol. 559, pp. 777-98, Sep 15 2004.
[30] J. M. Nerbonne, "Molecular Diversity of Ion Channels in the Mouse Heart," in *Cardiac Drug Development Guide*, M. K. Pugsley, Ed., ed Totowa, NJ Humana Press, 2003, pp. 245-269.
[31] H. Xu, W. Guo, and J. M. Nerbonne, "Four Kinetically Distinct Depolarization-activated K+ Currents in Adult Mouse Ventricular Myocytes," *The Journal of General Physiology,* vol. 113, pp. 661-678, 1999.
[32] Y. Rudy and J. R. Silva, "Computational biology in the study of cardiac ion channels and cell electrophysiology," *Quarterly reviews of biophysics,* vol. 39, pp. 57-116, 07/19 2006.
[33] V. E. Bondarenko, G. P. Szigeti, G. C. Bett, S. J. Kim, and R. L. Rasmusson, "Computer model of action potential of mouse ventricular myocytes," *Am J Physiol Heart Circ Physiol,* vol. 287, pp. H1378-403, Sep 2004.
[34] K. H. ten Tusscher, D. Noble, P. J. Noble, and A. V. Panfilov, "A model for human ventricular tissue," *Am J Physiol Heart Circ Physiol,* vol. 286, pp. H1573-89, Apr 2004.
[35] A. Mahajan, Y. Shiferaw, D. Sato, A. Baher, R. Olcese, L. H. Xie, *et al.*, "A rabbit ventricular action potential model replicating cardiac dynamics at rapid heart rates," *Biophys J,* vol. 94, pp. 392-410, Jan 15 2008.
[36] W. Guo, H. Xu, B. London, and J. M. Nerbonne, "Molecular basis of transient outward K+ current diversity in mouse ventricular myocytes," *J Physiol,* vol. 521 Pt 3, pp. 587-99, Dec 15 1999.

Dr. **Dongping Du** received the B.S. and M.S. degrees in electrical engineering from the China University of Mining and Technology, Beijing, China, and the Ph.D. degree in industrial engineering from the University of South Florida, Tampa, FL, USA. She is currently an Assistant Professor at the Department of Industrial Engineering, Texas Tech University, Lubbock, TX, USA. Her research focuses on nonlinear stochastic modeling and analysis of complex systems with applications in healthcare and systems engineering. Her research interests include complex system monitoring and control, biomedical informatics, computational cardiology, computer simulation and optimization, and big data analytics. Dr. Du has received the IBM Best Paper Award at the 2011 IEEE Annual Conference of Engineering in Medicine and Biology Society. Her research was also highlighted by the IEEE Journal of Biomedical and Health Informatics.

Dr. **Hui Yang** was born in Nanjing, China. He received the Ph.D. degree from the School of Industrial Engineering and Management, Oklahoma State University, Stillwater, OK, USA.
He is currently an Associate Professor at the Department of Industrial and Manufacturing Engineering, Pennsylvania State University, University Park, PA, USA. His research group has received multiple best paper awards from IEEE Annual Conference of Engineering in Medicine and Biology Society and Industrial Engineering Research Conferences. His research interests are sensor-based modeling and analysis of complex systems for the process monitoring/control, system diagnostics/prognostics, quality improvement, and performance optimization, with special focus on nonlinear stochastic dynamics, and the resulting chaos, multifractal, self-organization, long range dependence behaviors.

Dr. **Andrew R. Ednie** received his BS degree in Microbiology and Cell Science from the University of Florida. Following completion of his undergraduate degree, Andrew worked as an Analytical Chemist for a number of pharmaceutical companies. Andrew then earned his PhD degree from the Morsani College of Medicine at the University of South Florida in the department of Molecular Pharmacology and Physiology. After working as a post-doctoral scientist at the University of South Florida-Morsani College of Medicine, Andrew was promoted to and is currently a Research Assistant Professor of Neuroscience, Cell Biology, & Physiology at Wright State University, Dayton, OH. Andrew's major interests include elucidating the impact of post-translational modifications and protein-protein interactions on ion channel function and how these phenomena affect electrical excitability, conduction and electro-mechanical coupling in the heart and nervous system.

Dr. **Eric S. Bennett** received his BS degree in Applied & Engr. Physics from Cornell University, MS and PhD degrees in Biophysics from the University of Rochester. He is currently Chair of Neuroscience, Cell Biology, and Physiology at Wright State University, Dayton, OH, and is an active researcher in cardiac electrophysiology and molecular pharmacology. He is particularly interested in determining how cardiac excitability and conduction are controlled through posttranslational modifications of ion channels.

Techniques routinely used by his laboratory include primary and immortal cell culture methods, protein expression, protein biochemistry, basic confocal microscopy, molecular biological methods, and electrophysiological recordings. Studies on transgenic and knockout mice used to determine the in vivo role of channel glycosylation on ion channel function, on cardiac and neuronal action potentials, and on conduction using ECG, EEG, optical mapping, and in vivo electrophysiology measurements, are also done routinely in the lab. His lab has added transcriptomic and proteomic methods to determine N-glycan structures attached to neuronal and myocyte glycoproteins to the technical repertoire.